Ultrasonics 99 (2019) 105959

Contents lists available at ScienceDirect

Ultrasonics

journal homepage: www.elsevier.com/locate/ultras

Laser-ultrasonic nondestructive evaluation of porosity in particulate reinforced metal-matrix composites

N.B. Podymova[a,*], I.E. Kalashnikov[b], L.K. Bolotova[b], L.I. Kobeleva[b]

[a] Faculty of Physics, M.V. Lomonosov Moscow State University, Leninskie Gory, Moscow 119991, Russia
[b] A.A. Baikov Institute of Metallurgy and Material Science of Russian Academy of Sciences, Leninskii Prospect 49, Moscow 119991, Russia

ARTICLE INFO

Keywords:
Metal-matrix composites
Porosity
Broadband laser-ultrasonic spectroscopy
Longitudinal acoustic waves
Phase-velocity dispersion

ABSTRACT

In this work, we propose the laser-ultrasonic method for nondestructive evaluation of porosity in particulate reinforced metal-matrix composites fabricated by stir and *in-situ* reactive casting techniques. The method is based on the influence of porosity on dispersion of the phase velocity of longitudinal acoustic waves, which is measured by the broadband acoustic spectroscopy with laser excitation of ultrasound (laser-ultrasonic spectroscopy). We studied stir cast hypereutectic aluminum-silicon alloy A336 matrix composites reinforced with the SiC micro particles (3.3–13.5 vol%) and *in-situ* reactive cast Al/Al_3Ti composites reinforced with the Al_3Ti intermetallic particles (4–11.5 vol%). In the spectral range of 3–40 MHz, the phase-velocity dispersion in both types of composites was observed: the high-frequency velocity in the range of 20–40 MHz increases with the increase of the reinforcement content independent of porosity, whereas the low-frequency velocity in the range of 3–10 MHz decreases with the increase of porosity independent of the reinforcement content. As a result, the relative dispersion grows up with the increase in the composite porosity independent of the variation in the reinforcement content. The empirical dependence between the porosity in a scanning composite region and the relative phase-velocity dispersion in this region is approximated by the same unified function. For the first time, such unified porosity-phase velocity functional relationship is obtained for particulate reinforced metal-matrix composites completely different in fabrication techniques as well as in chemical composition and elastic properties of reinforcing particles.

1. Introduction

The development of composite materials is a perspective way among the methods of fabrication of new structural materials with enhanced mechanical and thermophysical properties. A wide variety of metal-matrix composites (MMCs) can be referred to these materials [1,2]. An optimal choice of composite components and its preliminary treatment make it possible to fabricate materials, which meet the requirements to particular service conditions (see, for example, [3–6]).

Currently, the most reliable MMCs are based on aluminum or magnesium and its alloys reinforced with different refractory ceramic particles. The most high-capacity and economical method of manufacturing of such MMCs is the stir casting technique [1]. However, some structural defects can appear in these materials resulting from its manufacturing process; the most common of them is porosity formed by gas bubbles and voids [7]. Porosity occurs in stir casting MMCs as a result of gases dissolved in the melt whose solubility decreases with decreasing temperature, physical entrainment of gases during stirring of reinforcing particles into the matrix melt, as well as because of shrinkage by solidification. In addition, quite poor wetting of ceramic particles by the matrix melt causes formation of voids at particle-matrix interfaces. Therefore, the porosity growth is associated with the increase in the content of reinforcing particles, that in turn results in debonding of particles from the matrix and subsequent decrease in the composite strength (see, for example, [8,9]).

To overcome these drawbacks, in the last decades the production of MMCs based on the chemical reactive casting technique is successfully developed. This technique consists in the *in-situ* synthesis of reinforcing phases in MMCs directly during the manufacturing process. These reinforcing phases in the form of refractory high-strength intermetallics originate as a result of the exothermal reaction between the matrix melt and the additives of reactively active metals or their oxides (see, for example, [10–12]). The intermetallic phases are thermodynamically stable, have a strong interfacial bond with the matrix due to the better lattice conformity, and are free of any contaminations of interfacial boundaries. In addition, the possibility of alteration of the chemical-

* Corresponding author.
E-mail address: npodymova@mail.ru (N.B. Podymova).

https://doi.org/10.1016/j.ultras.2019.105959
Received 5 May 2019; Received in revised form 16 June 2019; Accepted 5 July 2019
Available online 05 July 2019

reaction conditions makes it possible to change the volume content, sizes and shapes of reinforcing intermetallic particles in such a way to enhance the mechanical and thermophysical properties of produced composite materials. The main drawback of the reactive casting is the possible non-uniform distribution and clustering of intermetallic particles, the appearance of some shrinkage porosity, and non-uniformly distributed porosity formed by gases dissolved in the liquid mixture and entrained in the material after solidification [11,12].

Since the influence of porosity on the strength of the casting MMCs is very critical, the development of the methods of quantitative nondestructive evaluation of the local porosity in such composites is of great importance both for improvement of its manufacturing process and for detection of local regions with increased porosity in a finished material before fabrication of products.

Currently, ultrasonic methods are the most widely used for quantitative nondestructive evaluation of porosity in composites because of its relative simplicity, safety and high sensitivity to the presence of voids and pores (gas bubbles) [13]. This is because of a strong influence of porosity on the attenuation coefficient and velocity of ultrasonic waves, since voids and pores scatter these waves very effectively. In particulate MMCs, the reinforcing particles are also scatterers of ultrasonic waves, therefore the attenuation coefficient increases both by the growth in the reinforcement content and porosity (see, for example, [14] and references sited therein). For quantitative evaluation of the porosity value in MMCs using the measured frequency-dependent ultrasonic attenuation coefficient, it is necessary to calculate the partial contribution of reinforcing particles into the total attenuation. This contribution strongly depends on the shape and sizes of particles and the ratio between these sizes and a probe ultrasonic wavelength [15,16]. A large number of models for calculations of the ultrasonic attenuation (scattering) coefficient in two-phase elastic solids and particulate composites were developed (see, for example, representative works [17–21]). However, the fundamental drawback of all these models is that they are only applicable for spherical particles or cylindrical elongated inclusions, whereas there are no real particulate MMCs with such “ideal” reinforcing content. Therefore, calculations of the ultrasonic attenuation coefficient in such materials using the mentioned models are practically impossible. In other words, it is not possible to calculate “reference ultrasonic attenuation” in a pore-free MMC material with the complex-shaped reinforcement content to extract from the actual measured attenuation in a given porous MMC specimen the contribution of attenuation caused solely by porosity.

At the same time, the phase velocity of ultrasonic waves in such particulate MMCs can be calculated using a number of developed theoretical models for the elastic moduli of quasi-isotropic and quasi-homogeneous particulate MMCs with arbitrary reinforcing particle geometry: the classical analytical micromechanical model for multiphase materials [22], the three-phase self-consistent model for determination of the effective shear modulus of a composite system [23], the model for the elastic modulus of a two component isotropic composite, which takes into account the three-dimensional nature of stress and strain coupling in the material [24]. These models can be used providing that the elastic properties and content of the matrix and reinforcing particles are known and the probing ultrasonic wavelength is much more than sizes of particles. For quite low particle contents ($< 10–15\%$), the calculation results obtained using different models practically coincide with each other. The Hashin–Shtrikman variational bound model [22] is successfully used in many works to calculate the elastic properties of particulate MMCs with various reinforcement types and contents. The results show good agreement with experimental data obtained using the measured phase velocities of longitudinal and shear ultrasonic waves (see, for example, [25–27]). It means that the mentioned models can be used for the theoretical calculations of ultrasonic velocities in the solid (pore-free) phase of real porous MMCs under study. The calculation results can serve as the “reference” data to reveal the solely influence of porosity on the actual velocities in these materials.

Another reason for the preferable use of the ultrasonic velocity in MMCs instead of attenuation for quantitative evaluation of porosity is that the immersion technique widely used for the precise measurements of ultrasonic attenuation requires knowing of the reflection and transmission coefficients of ultrasonic waves for a studied MMC specimen. These values depend on the acoustic impedance of the specimen, which in turn is determined by the ultrasonic velocity. Therefore, to obtain the absolute value of the ultrasonic attenuation coefficient the ultrasonic velocity should anyway be measured. In addition, some instability in the amplitude of the reference ultrasonic pulse influences on the measurement results of absolute attenuation, whereas this instability has no impact on the measurement results of the phase velocity.

There are many theoretical and empirical models for the dependence of ultrasonic velocities on porosity. They are based on theories of the dependence of the elastic moduli on porosity [28–30], on structural models using an electro-acoustical analogy [31], or on the ultrasonic-wave scattering theory in porous media (see, for example, [32]). A modified theory of the dependence of ultrasonic velocities on porosity based on the Young’s modulus dependence on porosity assuming oblate spheroidal-shaped pores was proposed in [33]. All the mentioned theories accurately describe the experimental results for sintered single-phase metals and ceramics providing that the pore aspect ratio is known. However, they are very sensitive to the aspect ratio of pores and its orientation with respect to the reference ultrasonic beam and therefore are not applicable for particulate MMCs with arbitrary pore geometries.

The authors of [34] were probably the first who experimentally observed ultrasonic phase-velocity dispersion of longitudinal ultrasonic waves in carbon fiber reinforced plastic (CFRP) laminates with different porosities. It was found that in a frequency range of 3–8 MHz, the increase in porosity leads to the increase in relative velocity dispersion as compared with pore-free CFRPs. The same phenomenon in CFRP laminates was observed and quantitatively analyzed in recent works [35,36]. In [36], it was found that the increase in porosity leads to the increase in relative phase-velocity dispersion in a frequency range of 1–10 MHz independently on the volume content of the composite components.

In this work, we study the influence of porosity on the phase-velocity dispersion of longitudinal ultrasonic waves in particulate MMCs fabricated by stir and *in-situ* reactive cast techniques and having different contents of reinforcing ceramic or intermetallic particles and porosities. For this purpose, we use the laser-ultrasonic spectroscopy method described in detail in [35,36] and compare the experimental results with the phase velocity theoretically calculated using the Hashin-Shtrikman model [22]. In our opinion, the main advantage of laser excitation of ultrasound as compared with piezoelectric excitation is the ratio of the highest and the lowest frequencies of the spectral bandwidth of laser-induced ultrasonic pulses [36], which can be 10–20 times higher than that for piezoelectric transducers. This makes it possible to observe occurrence of dispersion of ultrasonic waves in a wide frequency range, which could probably not be revealed with the conventional piezoelectric transducers because of its limited bandwidth. This work continues our studies being started in [37] with the aim to find out, if porosity is the main factor affecting the phase-velocity dispersion in particulate reinforced MMCs independently of their fabrication technique (stir or *in-situ* reactive casting), chemical composition, and elastic properties of reinforcing particles (SiC or Al_3Ti). The goal of this work is to derive the empirical relation between phase-velocity dispersion in the megahertz frequency range and porosity in two completely different types of particulate reinforced MMCs, which can be used for ultrasonic quantitative nondestructive evaluation of porosity in such materials.

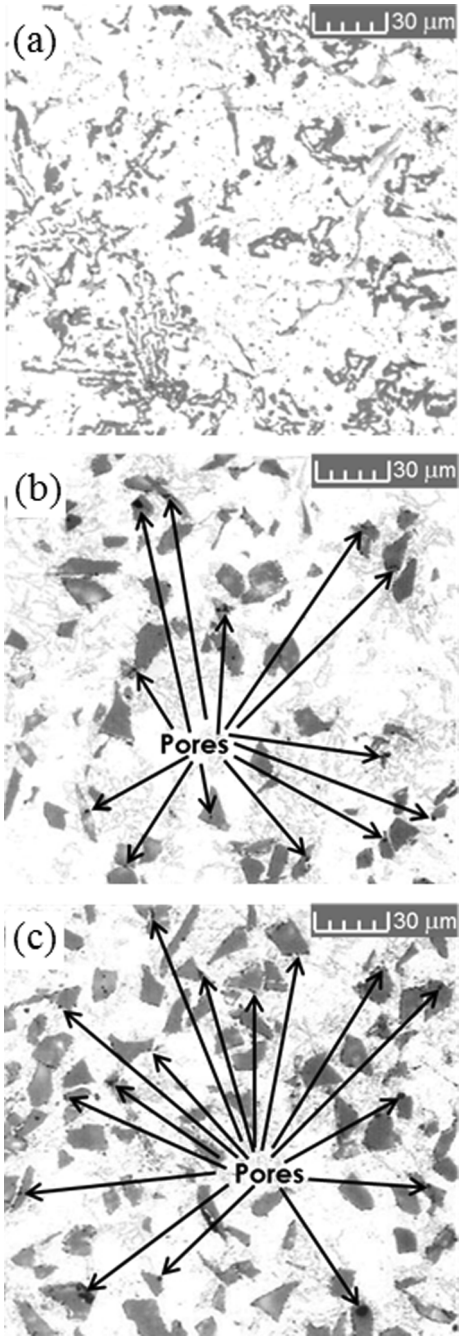

Fig. 1. Optical microscopy images: (a) A336 matrix specimen; Al/SiC composite specimen with (b) 6.7 vol% and (c) 13.5 vol% of SiC particles.

2. Materials and methodology

2.1. Stir-cast particulate metal-matrix composites

The first series of MMC specimens (#1, further specified as Al/SiC composites) was manufactured by the conventional stir casting technique, the matrix was the hypereutectic aluminum-silicon alloy AlSi13Mg1CuNi (A336) [38] reinforced by SiC particles with an average size of 14 μm. Three studied types of MMCs corresponded to three different contents of SiC (in vol%): 3.3; 6.7 and 13.5. All specimens were prepared as the plane-parallel fine-grinded disks with thickness $H = (5 \pm 0.005)$ mm and diameter $D = (50 \pm 0.1)$ mm. For both specimen sides, the maximum deviation from perfect flatness was estimated at a level of ± 5 μm.

Fig. 1 shows representative optical microscopy images of the "pure" A336 matrix without any reinforcement and the Al/SiC composite specimens with 6.7 vol% and 13.5 vol% of SiC.

The matrix is the crystallized alloy of the two-component eutectic (Al-Si) and multi-component eutectics with the intermetallic phases of Mg_2Si and $CuAl_2$ [38]. They form mutually embedded loops and dendrites, which look like a fine-dispersed mixture on the optical image. Fig. 1(a) shows that the matrix is practically pore-free. In the composite specimen, the reinforcing SiC particles depicted on Fig. 1(b) as grey lamellas are practically uniformly distributed and pores are mainly observed at the particle-matrix interfaces.

Porosity content P in the composite specimens averaged over their entire volume is determined as

$$P = (1 - \rho/\rho_0) \times 100\%, \quad (1)$$

where actual specimen density ρ is measured using hydrostatic weighing in distilled water (Archimedes' principle), density ρ_0 of the pore-free composite is calculated using the rule of mixtures with the known densities of A336 and SiC and their volume contents in the specimen:

$$\rho_0 = \sum_i n_i \rho_i, \quad (2)$$

where subscript "i" refers to the matrix ($i = 1$) or SiC ($i = 2$). The density of SiC is known [39]: $\rho_2 = 3.19 \times 10^3/m^3$, the density of A336 was taken as the measured density of the pore-free matrix specimen described above: $\rho_1 = 2725\ kg/m^3$. The measurement error of the specimen mass was about 2 mg, which together with the errors in the specimen dimensions resulted in the error of about $14\ kg/m^3$ for the specimen densities.

The technological parameters of all Al/SiC specimens under study are summarized in Table 1, where the first number in the specimen notation refers to the composite series (#1). One can see that the growth of SiC content leads to the increase of porosity P due to origin of pores (gas bubbles) at the particle-matrix interfaces.

Table 1
Technological parameters of Al/SiC composite specimens.

Specimen #	Volume content of components, n_i		Calculated density ρ_0, kg/m^3	Measured density ρ, kg/m^3	Porosity P, %
	A336	SiC			
1–0	1.000	0.000	2725	2725 ± 14	–
1–1	0.967	0.033	2740	2702 ± 14	1.38 ± 0.51
1–2	0.933	0.067	2756	2653 ± 14	3.75 ± 0.51
1–3	0.865	0.135	2788	2661 ± 14	4.54 ± 0.51

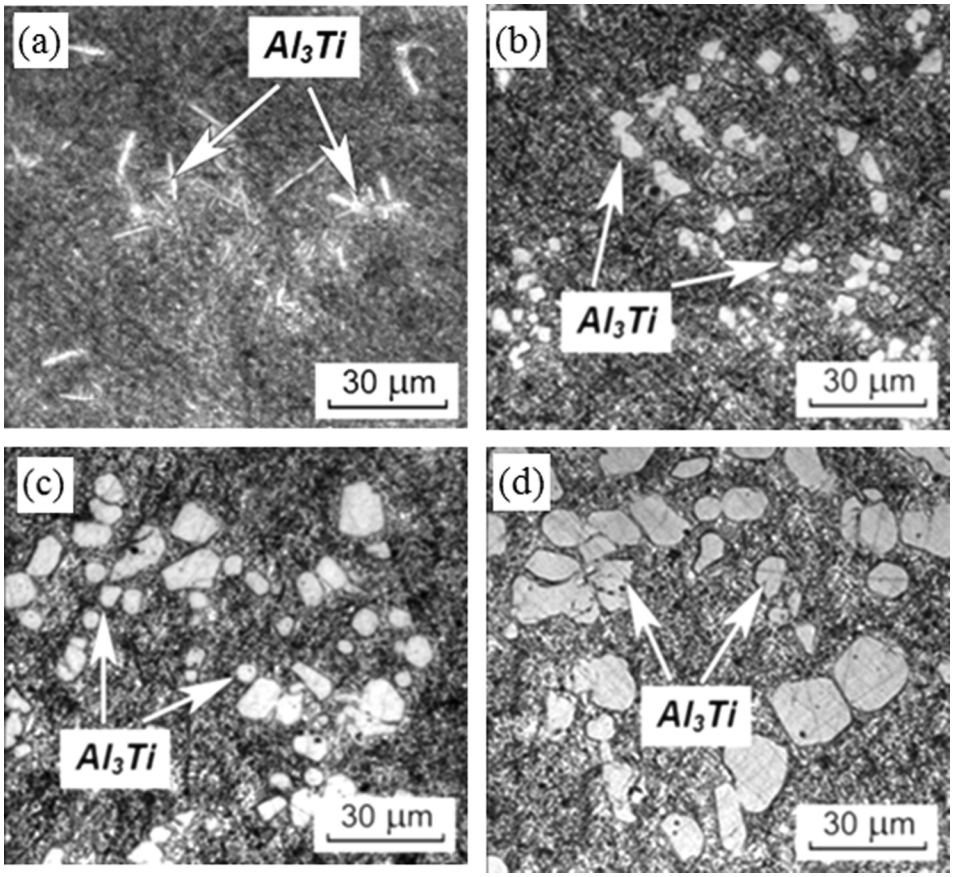

Fig. 2. Optical microscopy images of Al/Al_3Ti composite specimens manufactured by different holding times of the Al melt - Ti powder mixture before pouring: (a) 2, (b) 30, (c) 60, and (d) 90 min.

2.2. Reactive-cast particulate metal-matrix composites

The second series of MMC specimens (#2, further specified as Al/Al_3Ti composites) was manufactured by the mechanical stirring of 3 vol % of the titanium powder with the mean particle size of 200–400 μm into the melt of aluminum Al 1199 (the standard of the Aluminum Association). The mixture was heated up to 750 °C, stirred during 1 min and then hold at this temperature before pouring into graphite molds. The holding time τ_h was varied for four different specimens and was 2, 30, 60 and 90 min, respectively.

The insertion into the aluminum melt of reactively active titanium causes the exothermal reaction which results in in-situ formation of intermetallic Al-Ti phases according to the Al-Ti phase diagram [40]. For our experimental conditions, namely the melt temperature and the weight content of Ti, titanium trialuminide (Al_3Ti) is preferably synthesized and its maximum volume content reaches 11.5–12% (see, for example, [11,12,40–42]). Fig. 2 shows representative optical microscopy images for four Al/Al_3Ti composite specimens corresponding to four different holding times τ_h. The increase of τ_h leads to the transformation of needle-like Al_3Ti inclusions into block-like and to the increase in the volume content and mean size of Al_3Ti particles. For the holding time τ_h = 90 min, these parameters reach maximum values, 11.5 vol%, and 13.5 μm, respectively. Similar to Al/AlSiC composites, all Al/Al_3Ti specimens were prepared as the plane-parallel fine-grinded disks with thickness $H = (5 \pm 0.005)$ mm, diameter $D = (50 \pm 0.1)$ mm, and the maximum deviation of both specimen sides from perfect flatness was estimated at a level of ± 5 μm.

The corresponding structural parameters of Al/Al_3Ti composites were calculated in [42] and are shown in Table 2. The volume content n_{Ti} of unreacted titanium is calculated assuming that its entire initial volume is spent to formation of the maximum volume content of Al_3Ti (11.5%): $n_{Ti} = n_{0Ti}(1 - n_{Al_3Ti}/0.115)$, where n_{0Ti} = 3% is the initial volume content of titanium. The geometry and dimensions of all Al/Al_3Ti specimens was the same as for Al/SiC specimens (see Section 2.1). Porosity content P in the composite specimens averaged over their entire volume was determined with formula (1) using the actual

Table 2
Technological parameters of Al/Al_3Ti composite specimens.

Specimen #	Holding time τ_h, min	Volume content of components, n_i			Calculated density ρ_0, kg/m^3	Measured density ρ, kg/m^3	Porosity P, %
		Al	Ti	Al_3Ti			
2–0	–	1.000	0.000	0.000	2689	2687 ± 14	< 0.1
2–1	2	0.94	0.02	0.04	2751	2741 ± 14	0.36 ± 0.51
2–2	30	0.929	0.016	0.055	2753	2685 ± 14	2.47 ± 0.51
2–3	60	0.902	0.006	0.092	2762	2725 ± 14	1.34 ± 0.51
2–4	90	0.885	0.000	0.115	2766	2748 ± 14	0.65 ± 0.51

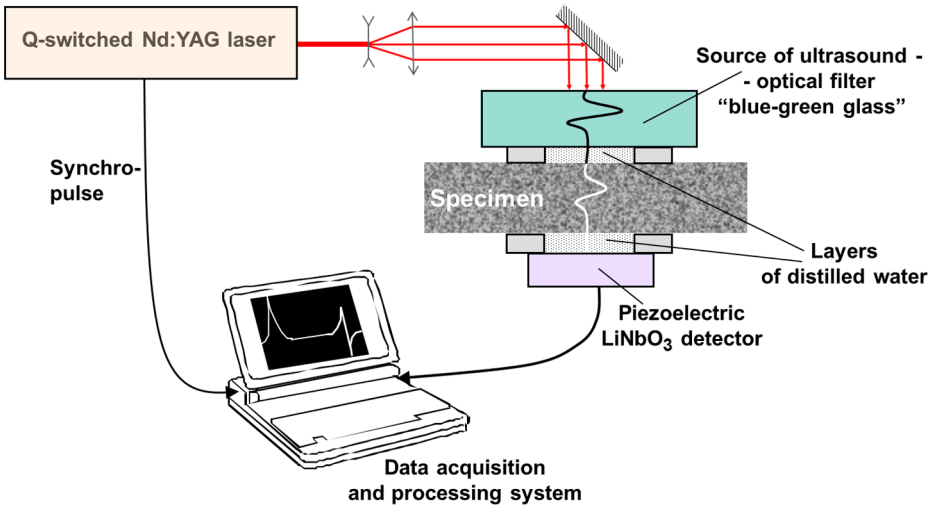

Fig. 3. Laser-ultrasonic spectroscopy setup.

specimen density measured by hydrostatic weighing in distilled water and density ρ_0 calculated with expression (2), in which subscript "i" refers to aluminum ($i = 1$), titanium ($i = 2$), and Al_3Ti ($i = 3$). The densities of these components are [39,41]: $\rho_{Al} = 2689\,kg/m^3$, $\rho_{Al_3Ti} = 3360\,kg/m^3$, and $\rho_{Ti} = 4505\,kg/m^3$.

It can be seen from Table 2, that the non-monotonic change of the specimen porosity is observed by the increase of the holding time. Probably, this is caused by the presence of gases dissolved in the liquid mixture; the gas concentration can grow up by the increase of the exothermal reaction duration. During the holding times of 30 and 60 min, these gases have not enough time to reach the mixture surface and remain entrapped in the crystallized material. By the increase of the holding time up to 90 min, all dissolved gases have time to reach the surface and escape the mixture, therefore the density of sample #2–4 grows up in accordance with the growth of the volume content of Al_3Ti.

2.3. Laser-ultrasonic spectroscopy method

The experimental setup of the broadband acoustic spectroscopy with laser thermoelastic excitation and piezoelectric detection of ultrasonic pulses is shown in Fig. 3 and is similar to that described in [36] except for some technical modifications. We used the same Q-switched Nd:YAG laser with the nearly Gaussian temporal profile with the characteristic pulse duration (pulse width) of 10–11 ns, but added an optical system consisting of convex and concave lenses to form the laser beam with a nearly Gaussian lateral intensity distribution with characteristic radius $a_0 \approx 5$ mm on the surface of a source of ultrasound (optoacoustic (OA) source). As this OA source, we used a plane-parallel polished plate of the optical filter "blue-green glass" with an acoustically free surface [43]. The light absorption coefficient for this filter at the operating laser wavelength is $\mu = 130–140\,cm^{-1}$, which makes it possible to effectively excite ultrasonic pulses with the spectral band ranging from 1–2 to 40–50 MHz and satisfy condition $a_0\mu \gg 1$, that in turn determines the nearly plane wave front of the excited reference ultrasonic beam [43]. The characteristic radius of this beam coincides with that of the laser beam and is equal to a_0.

Broadband ultrasonic pulses are received by a specially designed piezoelectric detector based on a Z-cut $LiNbO_3$ single crystal (thickness 30 μm, diameter 2 mm). Its resonance frequency is about 120 MHz, but some damping and operating in an open-circuit mode allowed us to obtain a quite flat amplitude-frequency response in a frequency range below the resonance. The used assembly of the detector with a charge preamplifier had the maximum low-frequency sensitivity of about 0.8 V/bar and the operational bandwidth 1–80 MHz at the $1/e$ level. Acoustic contacts between the OA source, specimen, and piezoelectric detector were provided with two 3-mm immersion layers of distilled water. Electrical output signals from the detector are acquired by a 12-bit analog-to-digital converter (ADC) with a sampling rate of 200 Msamples/s and processed via PC. The start of the ADC is synchronized with the instant of laser pulse emission.

Fig. 4 shows time profile along with amplitude and phase spectra of the reference ultrasonic pulse, which passed only through two 3-mm immersion water layers (without any studied specimen). A high stability of the temporal profile of reference ultrasonic pulses and operational parameters of the detection and acquisition system provide the minimum signal-to-noise ratio of our experimental setup at the level of approximately 5×10^{-4}.

Dispersion of the phase velocity of longitudinal acoustic waves, $C(f)$, is calculated using the phase spectrum of the reference ultrasonic pulse, $\phi_0(f)$, and that of the pulse passed through the specimen, $\phi(f)$:

$$C(f) = \frac{2\pi f H}{\phi(f) - \phi_0(f)}. \tag{3}$$

Here, f is the ultrasonic frequency, both $\phi_0(f)$ and $\phi(f)$ are already continuous phase spectra obtained using the standard phase unwrapping code [34], in which corresponding addition of term $\pm 2\pi n$ (n is an integer) is programmed in such a way to eliminate the ambiguity of the phase spectrum calculated from the arctangent function. The ADC was encoded to record these pulses in the corresponding time windows determined by the pulse time-of-flight through the acoustic path. Before the ultrasonic spectra of all pulses and phase-velocity dispersion were calculated, correction of frequency-dependent diffraction was made with the expression describing the diffraction transformation of broadband ultrasonic pulses ((2.47) in [43]).

The proposed laser-ultrasonic method makes it possible to measure the ultrasonic phase velocity averaged over the scanning specimen region. This region is approximately cylindrically-shaped providing that diffraction in the specimen is weak (see below Section 3); its diameter corresponds to that of the incident reference ultrasonic beam (≈ 5 mm) and the height is equal to the specimen thickness. Therefore, estimation of porosity averaged over this region is realized with the measured velocity. If the reference ultrasonic beam is shifted to impinge a specimen region with another porosity level, the measured phase velocity determined by "local" porosity in this particular scanning region will be different.

3. Results and discussion

It can be seen from Figs. 1 and 2 that the particle distribution in both types of composite specimens is quite uniform. This allows one to

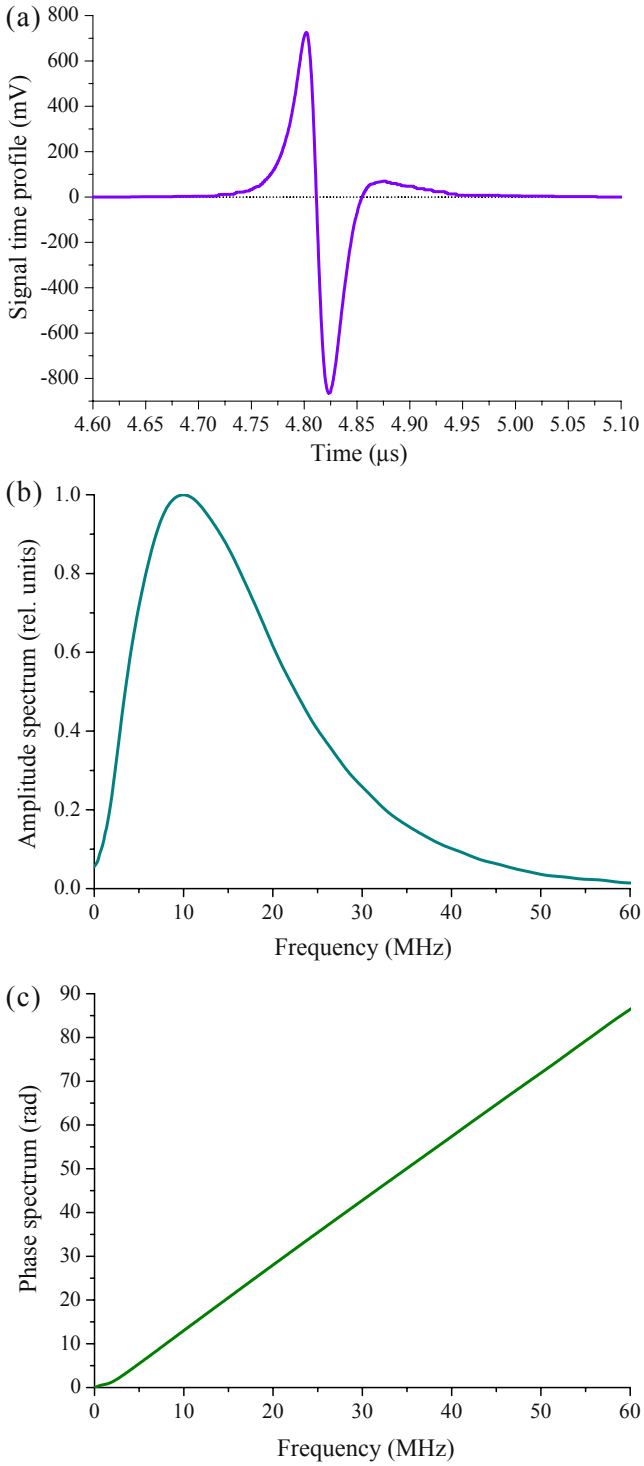

Fig. 4. Reference laser-induced ultrasonic pulse: (a) time profile, (b) amplitude, and (c) phase spectrum.

consider the studied specimens as acoustically isotropic. Figs. 5 and 6 show examples of time profiles, amplitude, and phase spectra of ultrasonic pulses passed through the Al/SiC and Al/Al_3Ti composite specimens, respectively. For comparison, the reference-pulse amplitude spectrum is also shown in Figs. 5b and 6b (right *Y* axes). Clearly, it is considerably wider than spectra of pulses passed through all studied specimens. The absence of any noise in the reference amplitude and phase spectra practically up to 60–70 MHz along with a quite large spectral amplitude at 40 MHz (about 10% of the maximum) provide the

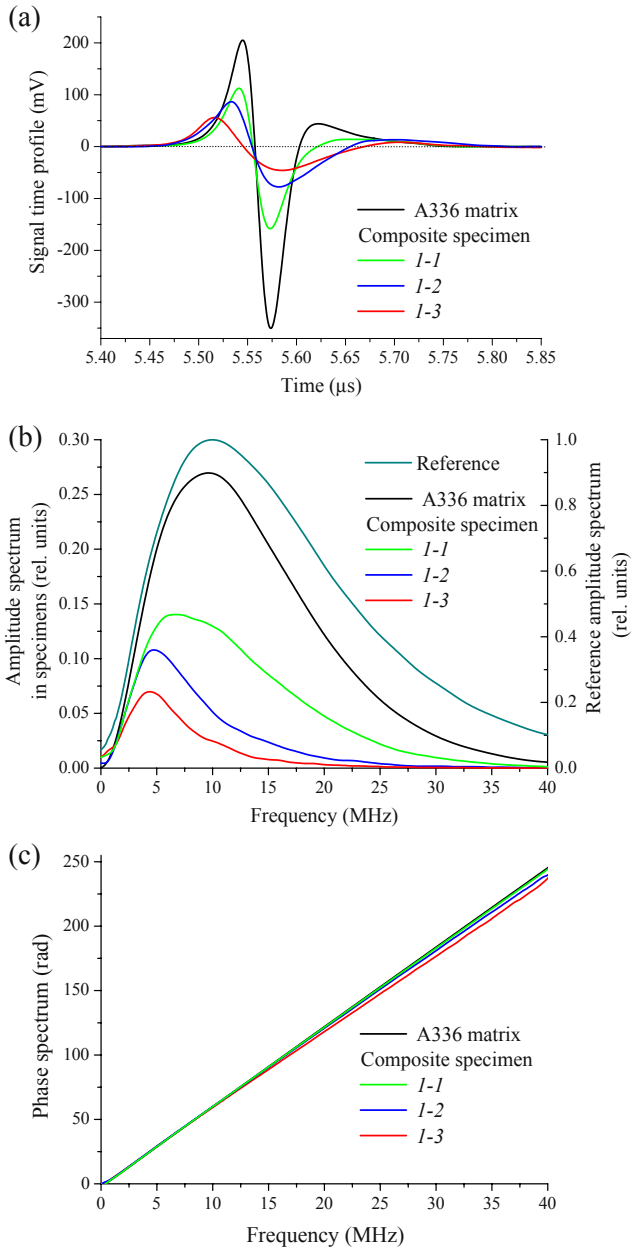

Fig. 5. Examples of (a) time profiles, (b) amplitude and (c) phase spectra of ultrasonic pulses passed through the Al/SiC composite specimens with different SiC contents and porosities.

possibility of reliable measurements of the phase velocity in the specimens at least up to 40 MHz.

In all specimens, measurements of the phase velocity were carried out in five randomly selected regions located at distances of about 10 mm from each other. For each specimen, the velocity variation in different regions did not exceed 10 m/s. Fig. 7 shows dependences $C(f)$ in Al/SiC and Al/Al_3Ti composite specimens calculated using expression (3) and averaged over five regions in each specimen. For frequencies $f < 3$ MHz, the phase velocity were not determined because of relatively high errors caused by significant diffraction of low-frequency ultrasonic harmonics. For $f > 40$ MHz, this velocity was also not determined since the amplitude of the transmitted ultrasonic harmonics at these frequencies was of the order of the noise level due to high attenuation in the specimens. In the operating frequency range of 3–40 MHz, the relative error for $C(f)$ depends on the signal-to-noise ratio for spectral amplitudes of each harmonic of the ultrasonic pulse

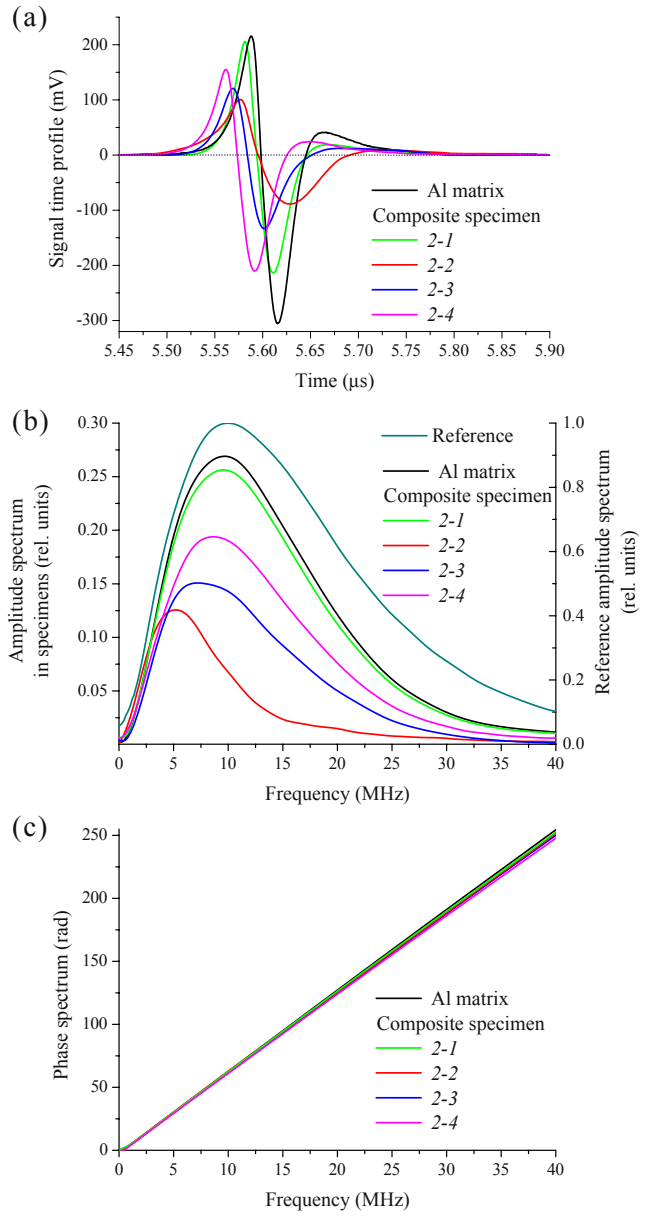

Fig. 6. Examples of (a) time profiles, (b) amplitude and (c) phase spectra of ultrasonic pulses passed through the Al/Al_3Ti composite specimens with different Al_3Ti contents and porosities.

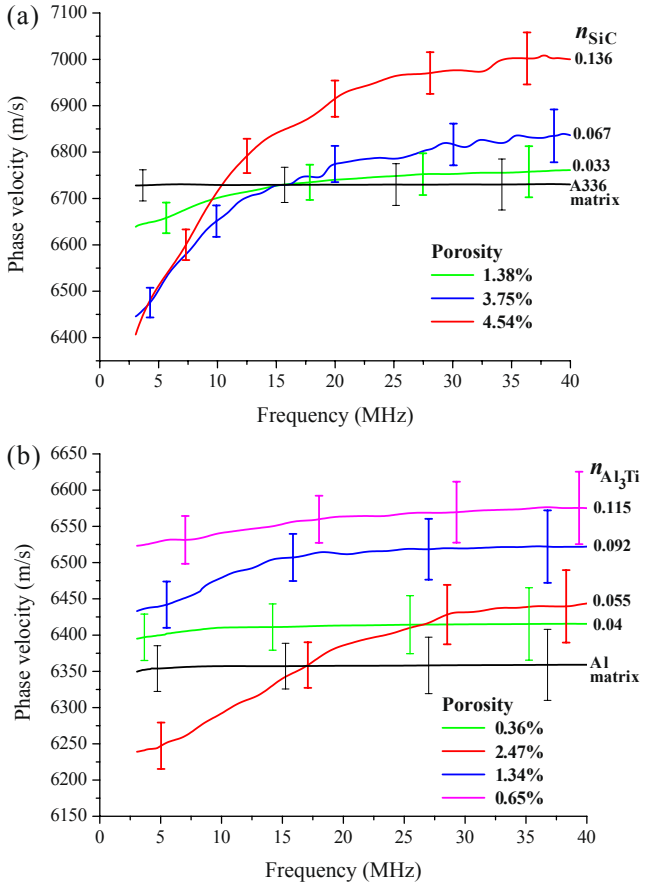

Fig. 7. Frequency dependences of phase velocity of longitudinal acoustic waves in (a) Al/SiC and (b) Al/Al_3Ti composite specimens with different reinforcing particle contents and porosities.

and on the measurement accuracy for the specimen's thickness. An additional error could be caused by a small variation of the thickness of water layers between the blue-green glass, specimen, and detector by arrangement of a specimen after recording of the reference ultrasonic pulse (without any specimen). The maximum deviation from perfect flatness for both specimen sides (± 5 μm) can cause deflection of the ultrasonic beam in a specimen at a maximum angle of about $5 \cdot 10^{-4}$ rad estimated for oblique incidence of the reference ultrasonic beam to the water-composite interface. This possible deflection was taken into account by estimations of the total relative measurement error for the phase velocity. As a result, this error is estimated at the level of 0.5–0.8% in the operating frequency range. In Fig. 7, several uncertainty bounds are shown, which correspond to the minimum and maximum errors for $C(f)$ as described above.

Since the diameter of the reference ultrasonic beam (10 mm) is practically 5 times more than the detector aperture (2 mm), the losses of the acoustic energy on the beam axis are detected and the use of expression (3) is rightfully. These losses are mainly caused by ultrasonic scattering on the structure inhomogeneities (particles and pores). Since their characteristic sizes (tenths of microns) are much less than the ultrasonic wavelengths in the operating frequency range (λ_u = 168 μm – 2.2 mm; for estimations of λ_u we took C = 6700 m/s), the Rayleigh scattering is realized. In this case, forward ultrasonic scattering is predominant [17] and the possible influence of 3D scattering on the phase-velocity dispersion is negligible. In addition, in this frequency range the influence on the true physical dispersion of so-called geometrical dispersion [44] caused by diffraction is also very weak. This is because of diffraction frequency f_{difr} (the maximum frequency, at which this effect is noticeable) calculated as $f_{difr} = HC/\pi a_0^2$ [43] is about 0.4 MHz for our experimental conditions, which is far beyond of our operating frequency range. Therefore, the phase-velocity dispersion observed in Fig. 7 is determined by ultrasonic scattering on reinforcing particles and pores in the studied composites.

For both types of composites, practically no phase-velocity dispersion was observed in the "pure" matrix (A 336 and Al) without any reinforcement. For Al/SiC composites (Fig. 7a), the phase velocity increases by the growth of SiC content n_{SiC} in spite of the growth of porosity P, but this increase is observed only in the high-frequency range (f > 20 MHz). The opposite situation takes place in the low-frequency range (f < 10 MHz) - the phase velocity decreases by the growth of porosity P in spite of the growth of n_{SiC}. It means that the porosity content P in the studied specimens causes occurrence of the phase-velocity dispersion of longitudinal acoustic waves: value $\Delta C = C_{max} - C_{min} \neq 0$, where $C_{min} = C$ (3 MHz) and $C_{max} = C$(40 MHz) are the minimum and maximum velocities for each specimen in the operating range 3–40 MHz. The parameter ΔC is the highest for

specimen #1–3 with the maximum porosity.

For Al/Al_3Ti composites (Fig. 7b), the growth of porosity is not associated with the increase of the reinforcing content (see Section 2.2). For low-porous specimens #2–1 (P = 0.36%) and #2–4 (P = 0.65%), practically no variations of velocity with frequency are observed within the accuracy limits. The absolute value of C is the largest in the entire operating frequency range for specimen #2–4 with the highest content of Al_3Ti particles, as it follows from the increase of elastic moduli of MMCs with the growth of the reinforcement content [22]. As well as for Al/SiC composites, parameter ΔC characterizing the phase-velocity dispersion is the highest for specimen #2–2 with the maximum porosity (P = 2.47%).

The phenomenon of the velocity dispersion of longitudinal acoustic waves in a porous material was theoretically analyzed in [45] using the mathematical analogy between plane wave propagation in a solid with voids and axial wave propagation along a circular cylindrical rod with radial shear and inertia. The main idea is that in a solid with voids, an initial longitudinal wave is transformed into a dispersive wave, which propagates with a lower velocity due to dilatational inertia around voids. The corresponding value of the velocity dispersion depends on the porosity content and on the ratio of pore sizes and ultrasonic wavelengths.

For quantitative characterization of porosity in the studied MMCs, we proposed to consider relative velocity dispersion $(C_{max} - C_{min})/C_{theor} = \Delta C/C_{theor}$, where C_{theor} is the theoretically calculated phase velocity of longitudinal acoustic waves in the corresponding pore-free composite. We believe, that this relative dispersion is solely determined by porosity, since (*i*) for low-porous specimens $\Delta C \approx 0$ and (*ii*) division of ΔC by C_{theor} eliminates the partial influence of reinforcing contents on the absolute velocity values. To calculate C_{theor}, we used the Hashin-Shtrikman model [22] for the variational lower bounds of the elastic moduli of a multiple-phase composite, since just these bounds provide the results closest to the experimentally obtained elastic moduli for various types of particulate MMCs [25–27]. For C_{theor}, we used the well-known expression $C_{theor} = \sqrt{(K + 4/3G)/\rho_0}$, where K and G are the bulk and shear moduli of the pore-free composite and ρ_0 is its density. To calculate K and G for Al/SiC two-phase composite, we used expressions (4.1)–(4.4) from [22], and for Al/Al_3Ti composite, we used expressions (3.37)–(3.42) and (3.44)–(3.49) from the same work for n = 3. The elastic moduli of all components of our composites used in the calculations are listed in Table 3, where $K = E/3(1 - 2\nu)^{-1}$. For Al_3Ti, the Young and shear moduli, as well as the Poisson's ratio depend on its crystal lattice type (tetragonal or cubic) and its values given in different references vary in quite wide ranges. Since in our composites the exact lattice type of Al_3Ti is not known, we used averaged values of the mentioned elastic parameters.

In Table 4, the summary data on the phase velocities together with porosity values for all studied composite specimens are shown. For both composite types, the difference between theoretically calculated C_{theor} and measured high-frequency C_{max} is quite small (< 100 m/s). It means that the high-frequency phase velocity of longitudinal ultrasonic waves is mainly determined by the elastic properties and volume content of the reinforcing particles and is practically independent of porosity.

For quantitative characterization of porosity in the studied MMC specimens, we plotted the relationship between porosity P and relative velocity dispersion $\Delta C/C_{theor}$ as dependence $P(\Delta C/C_{theor})$ for all specimens (Fig. 8, points). For two different types of composites, this empirical dependence can be fitted using the least-squares method by one and the same power function:

$$y = 0.996x^{0.732}. \quad (4)$$

The relative errors of the fitting parameters in expression (4) do not exceed 8%. Here, the x value corresponds to relative velocity dispersion $\Delta C/C_{theor}$ taken in percent and the y value corresponds to porosity P also taken in percent.

Functional dependence (4) obtained by fitting of the empirical data on the phase-velocity dispersion can be used as a "calibration curve" for ultrasonic quantitative evaluation of porosity P in stir cast Al/SiC and *in-situ* reactive cast Al/Al_3Ti composites for reinforcing particle contents up to 13–14 vol%. It is interesting to note that the dependence $P(\Delta C/C_{theor})$ is the same for different types of reinforcements with very different chemical composition and elastic properties. It means that the observed relative dispersion of the phase velocity is mainly governed by porosity in the studied particulate MMCs and is practically independent of the fabrication technique and of the specific type of reinforcing particles.

To validate the performance of the proposed technique, we used the derived "calibration curve" to evaluate porosity in an *in-situ* reactive cast Al/Al_3Ti composite specimen fabricated with the same technique described in Section 2.2, but with adding of 0.2 vol% of synthetic diamond nanoparticles of 50 nm in size [42]; specimen shape and thickness were the same as for all studied Al/Al_3Ti specimens. The diamond nanoparticles affected on acceleration of growth of Al_3Ti particles as compared with the composites described in Section 2.2, as well as on enhancement of tribological characteristics of the composite [42]. A representative optical microscopy image for such specimen manufactured by holding time τ_h = 30 min is shown in Fig. 9a. The volume content of Al_3Ti particles in this specimen was practically the same as in specimen # 2–2, but the mean particle size was larger because of a faster rate of Al_3Ti synthesis. Fig. 9b shows the phase-velocity dispersion curve measured in this specimen with the proposed laser-ultrasonic method. For this specimen, measured values C_{min} = 6142 m/s and C_{max} = 6478 m/s, calculated values C_{theor} = 6436 m/s and $\Delta C/C_{theor}$ = 5.22%; and corresponding porosity calculated with "calibration curve" (4) is $P = (3.34 \pm 0.27)$%. Here, the error is equal to the relative error of the fitting parameters in (4). Next, a cylinder of 1 cm in diameter was cut from the scanning region of this specimen and porosity of this cylinder was determined by hydrostatic weighing in distilled water, as it was made for all studied specimens. The porosity value was equal to 3.6%, which practically coincides with that determined using formula (4) taking into account the fitting error bounds. A higher porosity level in this composite as compared with specimen #2–2 is probably caused by the accelerated rate of the exothermal reaction of Al_3Ti synthesis.

Thus, the "blind" test experiment on a MMC specimen with porosity unknown in advance confirmed the validity of application of fitting function (4) proposed for the first time for nondestructive porosity evaluation in particulate reinforced MMCs manufactured with completely different processing techniques and containing different types of reinforcements.

Table 3
Elastic characteristics of components of studied MMCs.

Component	Young's modulus E, GPa	Shear modulus G, GPa	Poisson's ratio ν	Bulk modulus K, GPa	Reference
A 336	83.5	31.3	0.327	80.4	[46]
SiC	419.4	180.4	0.16	205.6	[25]
Al	70.6	26.3	0.34	73.6	Measured in this work with the method described in [46]
Ti	110	41.5	0.33	107.8	[39]
Al_3Ti	216	93	0.23	133.3	[47,48]

Table 4
Porosity and phase velocities of longitudinal ultrasonic waves in studied MMC specimens.

Type	Specimen #	Porosity P, %	C_{min}, m/s	C_{max}, m/s	C_{theor}, m/s	ΔC, m/s	$\Delta C/C_{theor}$, %
Al/SiC	1–1	1.38	6639	6761	6794	122	1.80
	1–2	3.75	6446	6837	6893	391	5.72
	1–3	4.54	6407	7005	7101	598	8.42
Al/Al_3Ti	2–1	0.36	6395	6416	6402	21	0.33
	2–2	2.47	6239	6444	6429	205	3.19
	2–3	1.34	6433	6522	6497	89	1.37
	2–4	0.65	6523	6575	6540	52	0.80

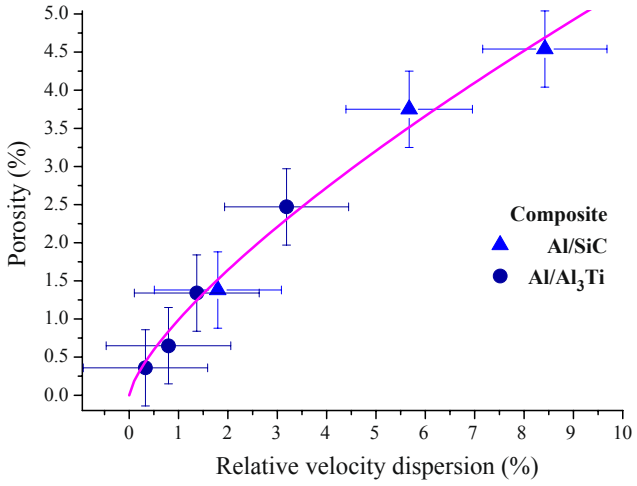

Fig. 8. Relationship between relative phase-velocity dispersion of longitudinal acoustic waves and porosity in stir cast Al/SiC and *in-situ* reactive cast Al/Al_3Ti composites. Points are the experimental results; solid curve is approximation function (4).

4. Conclusions

In this work, the laser-ultrasonic spectroscopy method for non-destructive evaluation of porosity in stir cast and *in-situ* reactive cast particulate-reinforced metal-matrix composites is proposed and realized. This method was used to study dispersion of the phase velocity of longitudinal acoustic waves in the composite specimens with different contents of reinforcing particles and porosities. Two different types of composites were studied: stir cast hypereutectic aluminum-silicon alloy A336 matrix composites reinforced with the SiC micro particles (volume contents 3.3–13.5%) and *in-situ* reactive cast Al/Al_3Ti composites with the Al_3Ti intermetallic particles (volume contents 4–11.5%). In the operating frequency range of 3–40 MHz, the phase-velocity dispersion was observed in the composite specimens of both types with porosities > 1%: the high-frequency velocity in the range of 20–40 MHz increases with the increase of the reinforcement content independent of porosity, whereas the low-frequency velocity in the range of 3–10 MHz decreases with the increase of porosity independent of the reinforcement content. As a result, the relative dispersion determined as the difference between the high- and low-frequency velocities normalized by the velocity theoretically calculated using the Hashin-Shtrikman model for the multi-phase quasi-isotropic composites, grows up solely by the porosity increase and is independent of the specific type and contents of reinforcing particles. We found that for two different types of composites, the empirical relation between the porosity in the scanning composite region and relative phase-velocity dispersion in this region is approximated by the unified power function. This function can serve as a "calibration curve" for quantitative nondestructive evaluation of porosity in the studied types of stir cast and *in-situ* reactive cast particulate-reinforced metal-matrix composites.

The novelty of this work is that the unified porosity-phase velocity functional relationship is obtained for the first time for particulate reinforced metal-matrix composites completely different in fabrication techniques as well as in chemical composition and elastic properties of reinforcing particles. Further development of the proposed laser-ultrasonic spectroscopy method together with the mechanical strength, fatigue life and wear tests of different types of particulate-reinforced metal-matrix composites seems to be promising for working out the quantitative design acceptance criteria for these materials with various porosity contents.

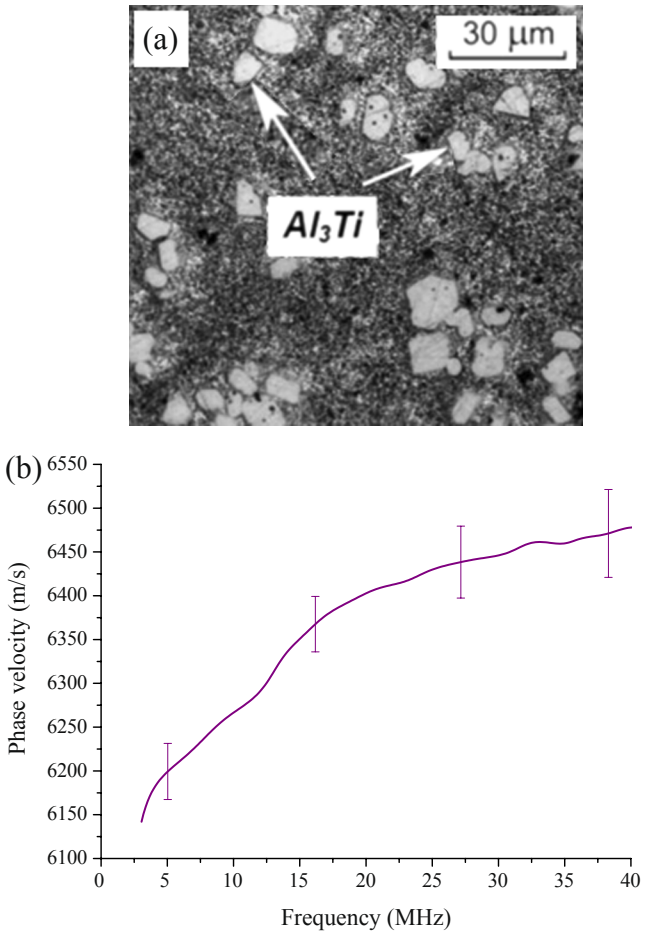

Fig. 9. (a) Optical microscopy image and (b) phase-velocity dispersion curve for the Al/Al_3Ti composite specimen manufactured with adding of 0.2 vol% of synthetic diamond particles of 50 nm in size by holding time τ_h = 30 min.

Acknowledgments

This work was supported by the Russian Foundation for Basic Research, project no. 18-58-00009 Bel-a.

References

[1] T.W. Clyne, P.J. Withers, An Introduction to Metal Matrix Composites, Cambridge University Press, Cambridge, 1995.
[2] K.U. Kainer, Basics of metal matrix composites, in: K.U. Kainer (Ed.), Metal Matrix Composites: Custom-made Materials for Automotive and Aerospace Engineering, Wiley-VCH Verlag GmbH & Co, Weinheim, 2006.
[3] I.A. Ibrahim, F.A. Mohamed, E.J. Lavernia, Particulate reinforced metal matrix composites – a review, J. Mater. Sci. 26 (1991) 1137–1156.
[4] D.J. Lloyd, Particle reinforced aluminium and magnesium matrix composites, Int. Mater. Rev. 39 (1994) 1–23.
[5] M.K. Surappa, Aluminium matrix composites: challenges and opportunities, Sadhana 28 (2003) 319–334.
[6] T.A. Chernyshova, L.I. Kobeleva, L.K. Bolotova, I.V. Katin, Structure and properties of hybrid composite materials, Russian Metallurgy (Metally) 3 (2013) 220–228.
[7] J. Campbell, Porosity, Complete Casting Handbook. Metal Casting Processes, Metallurgy, Techniques and Design, Butterworth-Heinemann, Elsevier, Amsterdam, 2015.
[8] P.N. Bindumadhavan, H.K. Wah, O. Prabhakar, Assessment of particle–matrix debonding in particulate metal matrix composites using ultrasonic velocity measurements, Mater. Sci. Eng. A 323 (2002) 42–51.
[9] C. Tekmen, I. Ozdemir, U. Cocen, K. Onel, The mechanical response of Al-Si-Mg/SiC_p composite: influence of porosity, Mater. Sci. Eng. A 360 (2003) 365–371.
[10] H. Fukunaga, X. Wang, Y. Aramaki, Preparation of intermetallic compound matrix composites by reaction squeeze casting, J. Mater. Sci. Lett. 10 (1991) 23–25.
[11] S.C. Tjong, Z.Y. Ma, Microstructural and mechanical characteristics of in situ metal matrix composites, Mater. Sci. Eng. R 29 (2000) 49–113.
[12] R.A. Varin, Intermetallic-reinforced light-metal matrix *in-situ* composites, Metall. Mater. Trans. A 33 (2002) 193–201.
[13] S.I. Rokhlin, D.E. Chimenti, P.B. Nagy, Physical Ultrasonics of Composites, Oxford University Press, Oxford, 2011.
[14] P. Mylavarapu, E. Woldesenbet, A predictive model for ultrasonic attenuation coefficient in particulate composites, Compos. Part B Eng. 41 (2010) 42–47.
[15] A. Vary, Material property characterization, in: P.O. Moore (Ed.), Nondestructive Testing Handbook. Ultrasonic Testing, ASTM, Columbus, 2007.
[16] Li Sun, Aiming Ji, Hu. Jialing, Canyan Zhu, Lijun Zhang, Jianfeng Yang, Yongsong Liu, Ling-Feng Mao, A method to measure the distance among scatters and the scatters' diameter in artificial composite materials, Ultrasonics 67 (2016) 70–75.
[17] C.F. Ying, R. Truell, Scattering of a plane longitudinal wave by a spherical obstacle in an isotropically elastic solid, J. Appl. Phys. 27 (1956) 1086–1097.
[18] V.K. Varadan, V.V. Varadan (Eds.), Acoustic, Electromagnetic and Elastic Wave Scattering – Focus on the T-Matrix Approach, Pergamon, New York, 1980.
[19] V.K. Kinra, A. Anand, Wave propagation in a random particulate composite at long and short wavelengths, Int. J. Solids Struct. 18 (1982) 367–380.
[20] S.K. Kanuan, V.M. Levin, F.J. Sabina, Propagation of elastic waves in composites with random set of spherical inclusions (effective medium approach), Wave Motion 40 (2004) 69–88.
[21] J.Y. Kim, On the generalized self-consistent model for the elastic wave propagation in composite materials, Int. J. Solids Struct. 41 (2004) 4349–4360.
[22] Z. Hashin, S. Shtrikman, A variational approach to the theory of the elastic behaviour of multiphase materials, J. Mech. Phys. Solids 11 (1963) 127–140.
[23] R.M. Christensen, K.H. Lo, Solutions for effective shear properties in three phase sphere and cylinder models, J. Mech. Phys. Solids 27 (1979) 315–330.
[24] A.J. Owen, I. Koller, A note on the Young's modulus of isotropic two-component materials, Polymer 37 (1996) 527–530.
[25] S. Santhosh Kumar, V. Seshu Bai, K.V. Rajkumar, G.K. Sharma, T. Jayakumar, T. Rajasekharan, Elastic modulus of Al–Si/SiC metal matrix composites as a function of volume fraction, J. Phys. D: Appl. Phys. 42 (2009) 175504–1–10.
[26] A.A. El-Daly, M. Abdelhameed, M. Hashish, A.M. Eid, Synthesis of Al/SiC nanocomposite and evaluation of its mechanical properties using pulse echo overlap method, J. Alloy. Compd. 542 (2012) 51–58.
[27] Yu Liu, Yongfeng Song, Xiongbing Li, Chao Chen, Kechao Zhou, Evaluating the reinforcement content and elastic properties of Mg-based composites using dual-mode ultrasonic velocities, Ultrasonics 81 (2017) 167–173.
[28] E.A. Dean, Elastic moduli of porous sintered materials as modeled by a variable–aspect–ratio self-consistent oblate-spheroidal-inclusion theory, J. Am. Ceram. Soc. 66 (1983) 847–854.
[29] A.K. Maitra, K.K. Phani, Ultrasonic evaluation of elastic parameters of sintered powder compacts, J. Mater. Sci. 29 (1994) 4415–4419.
[30] K.K. Phani, Porosity dependence of ultrasonic velocity in sintered materials – a model based on the self-consistent spheroidal inclusion theory, J. Mater. Sci. 31 (1996) 272–279.
[31] V.V. Polyakov, A.V. Golovin, Elastic moduli of porous metals, Phys. Met. Metallogr. 79 (1995) 147–149.
[32] C.M. Sayers, R.L. Smith, The propagation of ultrasound in porous media, Ultrasonics 20 (1982) 201–205.
[33] D.N. Boccaccini, A.R. Boccaccini, Dependence of ultrasonic velocity on porosity and pore shape in sintered materials, J. Nondestruct. Eval. 16 (1997) 187–192.
[34] H. Jeong, D.K. Hsu, Experimental analysis of porosity-induced ultrasonic attenuation and velocity change in carbon composites, Ultrasonics 33 (1995) 195–203.
[35] N.B. Podymova, A.A. Karabutov, Broadband laser-ultrasonic spectroscopy for quantitative characterization of porosity effect on acoustic attenuation and phase velocity in CFRP laminates, J. Nondestruct. Eval. 33 (2014) 141–151.
[36] Yu.G. Sokolovskaya, N.B. Podymova, A.A. Karabutov, Verification of the Kramers-Kronig relations between ultrasonic attenuation and phase velocity in a finite spectral range for CFRP composites, Ultrasonics 95 (2019) 37–44.
[37] N.B. Podymova, A.A. Karabutov, Combined effects of reinforcement fraction and porosity on ultrasonic velocity in SiC particulate aluminum alloy matrix composites, Compos. Part B Eng. 113 (2017) 138–143.
[38] J.R. Davis (Ed.), ASM Specialty Handbook: Aluminum and Aluminum Alloys, ASM International, 1993.
[39] I.S. Grigoriev, E.Z. Meilikhov, A.A. Radzig (Eds.), Handbook of Physical Quantities, CRC-Press, Boca Raton, 1997.
[40] V.T. Witusiewicz, A.A. Bondar, U. Hecht, S. Rex, T.Ya. Velikanova, The Al-B-Nb-Ti system: III. Thermodynamic re-evaluation of the constituent binary system Al-Ti, J. Alloys Compd. 465 (2008) 64–77.
[41] M. Yamaguchi, H. Inui, Al_3Ti and its $L1_2$ variations, in: J.H. Westbrook, R.L. Fleischer (Eds.), Intermetallic Compounds Principles and Practice, John Wiley & Sons Ltd., Chichester, 1994.
[42] T.A. Chernyshova, L.K. Bolotova, I.E. Kalashnikov, L.I. Kobeleva, P.A. Bykov, Effect of refractory nanoparticles on the structural modification of metal-matrix composites, Russian Metallurgy (Metally) 3 (2007) 236–241.
[43] V.E. Gusev, A.A. Karabutov, Laser Optoacoustics, American Institute of Physics, New York, 1993.
[44] A.M. Gavrilov, R.O. Sitnikov, Measurement of geometrical dispersion in a sound beam, Acoust. Phys. 52 (2006) 548–554.
[45] T.W. Wright, Elastic wave propagation through a material with voids, J. Mech. Phys. Solids. 46 (1998) 2033–2047.
[46] A.A. Karabutov, N.B. Podymova, L.I. Kobeleva, T.A. Chernyshova, Quantitative evaluation of the effect of porosity on the local Young's modulus of isotropic composites by using the laser optoacoustic method, Mech. Compos. Mater. 49 (2013) 411–420.
[47] C.L. Fu, Electronic, elastic, and fracture properties of trialuminide alloys: Al_3Sc and Al_3Ti, J. Mater. Res. 5 (1990) 971–979.
[48] M. Nakamura, K. Kimura, Elastic constants of TiAl3 and ZrAl3 single crystals, J. Mater. Sci. 26 (1991) 2208–2214.